Donor-Acceptor Pyridinium Salts for Photo-Induced Electron Transfer Driven Modification of Tryptophan in Peptides, Proteins, and Proteomes using Visible Light

Caleb R. Hoopes^{†a}, Francisco J. Garcia^{‡b}, Akash M. Sarkar^a, Nicholas J. Kuehl^a, David T. Barkan^b, Nicole L. Collins^a, Glenna E. Meister^b, Taylor R. Bramhall^b, Chien-Hsiang Hsu^b, Michael D. Jones^b, Markus Schirle^b, and Michael T. Taylor^a*

^aUniversity of Wyoming, Department of Chemistry, Laramie, WY 82071, United States

^bNovartis Institutes for Biomedical Research, 181 Massachusetts Ave, Cambridge, MA, 02138, United States Supporting Information Placeholder

ABSTRACT: Tryptophan (Trp) plays a variety of critical functional roles in protein biochemistry however, owing to its low natural frequency and poor nucleophilicity, the design of effective methods for both single protein bioconjugation at Trp as well as for in situ chemoproteomic profiling remains a challenge. Here, we report a method for covalent Trp modification that is suitable for both scenarios by invoking photo-induced electron transfer (PET) as a means of driving efficient reactivity. We have engineered biaryl Ncarbamoyl pyridinium salts that possess a donor-acceptor relationship which enables optical triggering with visible light whilst simultaneously attenuating the probe's photooxidation potential in order to prevent photodegradation. This probe was assayed against a small bank of eight peptides and proteins, where it was found that micromolar concentrations of probe and short irradiation times (10-60 min) with violet light enabled efficient reactivity towards surface exposed Trp residues. The carbamate transferring group can be used to transfer useful functional groups to proteins including affinity tags and click handles. DFT calculations and other mechanistic analyses reveal correlations between excited state lifetimes, relative fluorescent quantum yields, and chemical reactivity. Biotinylated and azide-functionalized pyridinium salts were used for Trp profiling in HEK293T lysates and *in situ* in HEK293T cells using 440 nm LED irradiation. Peptide level enrichment from live cell labelling experiments identified 290 Trp modifications, with an 82% selectivity for Trp modification over other π -amino acids; demonstrating the ability of this method to identify and quantify reactive Trp residues from live cells.

Introduction

The union of covalent protein modification chemistry with proteomic analysis has enhanced the molecular precision of drug discovery by enabling the target identification of small molecule therapeutics through activity-based protein profiling, the precision design of covalent inhibitors, and through the characterization of transient and dynamic aspects of a

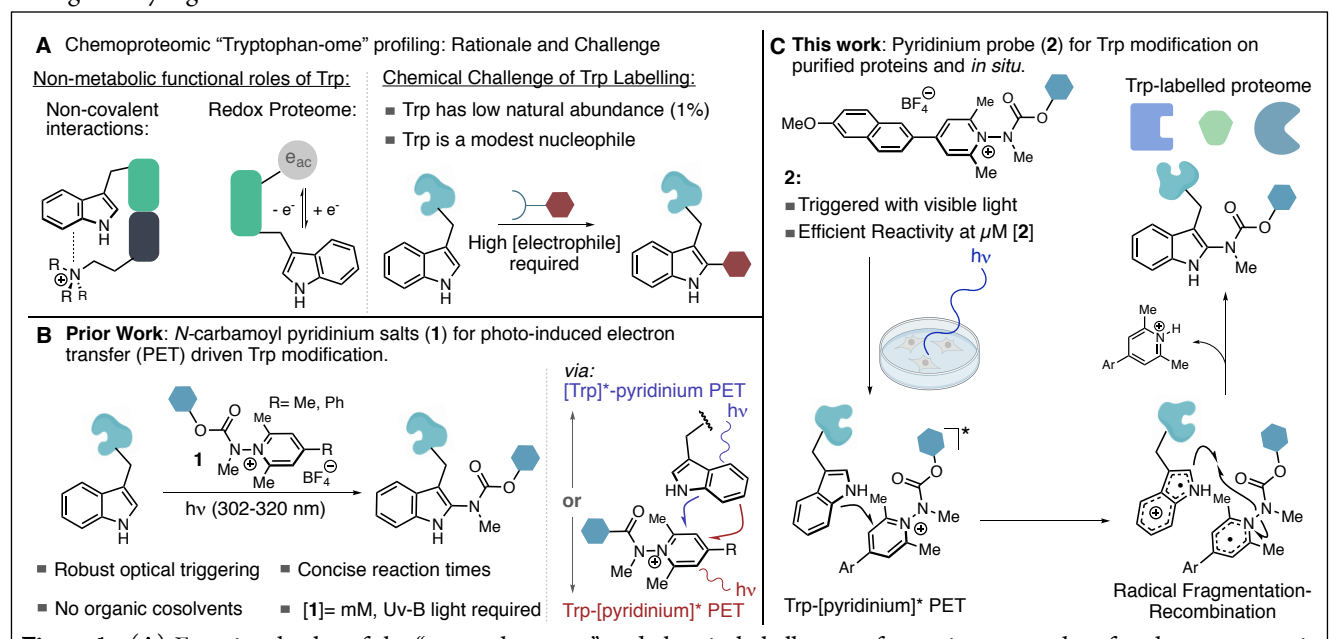


Figure 1. (**A**) Functional roles of the "tryptophan-ome" and chemical challenges of targeting tryptophan for chemoproteomic profiling. (**B**) Harnessing photo-induced electron transfer (PET) for Trp modification using *N*-carbamoyl pyridinium salts. (**C**) This work: Visible light activated probe for selective Trp modification in purified peptides and *in situ* proteomic profiling.

proteome¹. Recently, site-selective protein modification technologies have been adapted for use in broad spectrum chemoproteomic interrogation of a given reactive moiety (typically, an amino acid side-chain)2. This approach enables the characterization of reactive hotspots surrounding the moiety of interest. This information can then lead to the discovery of new sites of biological significance and, ultimately, the discovery of new druggable sites. Many chemoproteomic profiling strategies make use of either direct or insitu generated electrophiles which target either strongly nucleophilic species, such as cysteine^{2a-c}, or higher abundance residues of moderate to weak nucleophilicity such as lysine2df, serine/threonine^{2f}, tyrosine^{2g,h}, and aspartate/glutamate^{2i,h}. An elegant example from Chang and Toste targeted weakly nucleophilic, low abundance methionine residues in lysates^{2k}.

However, electrophilic approaches directed towards other functionally important residues, such as tryptophan (Trp), remain a persistent challenge. The challenge of chemoproteomic profiling of Trp stems from a combination of Trp's very low natural abundance and the modest nucleophilicity of its indole sidechain³. This combination necessitates that any Trp-selective electrophile would have to possess both sufficient kinetic competency and selectivity to label Trp (ideally *in situ*) in a complex proteome at low concentrations of reagent. As such, Trp has been the subject of many innovative labelling approaches, including through the use of sulfenyl chlorides^{4a,b}, metallocarbenoids^{4c,d}, nitroxides^{4e}, transition metal catalyzed processes^{4f}, oxidative strategies^{4g} and photoredox catalysis^{4h}. Whilst comprising an elegant body of work, these methods would require significant adaptation for use as chemical probes for Trp residues in situ. In 2003, Nishimura used a 2-nitrobenzenesulfenyl chloride isotopologue for chemoselective Trp modification in rat serum; resulting in the identification of three tryptic peptides harboring a Trp modification^{4b}. In 2007, Leitner reported an approach that enabled enrichment of Trp-containing peptides through reversible condensation of malondialdehyde onto the Trp-indolic N-H followed by enrichment on hydrazide-derivatized beads; an approach that enabled the identification of nine proteins from yeast lysates⁴ⁱ. Whilst demonstrating the premise, these strategies required either predenaturation of proteins and labelling performance under acidic conditions or the use of unselective chemistries; precluding the use of these methods in more complex environments.

Despite these challenges, chemoproteomic profiling of Trp presents a unique chemical challenge and opportunity (Figure 1A). Trp is widely dispersed throughout the proteome and is also relatively evenly distributed between surface exposed and buried positions⁵. Trp possesses the most electron-rich π -system of the naturally occurring amino acids; a property that enables Trp to engage in electrostatically-driven non-covalent interactions such as π - π , cation- π , and

X-H- π interactions, as well as through H-bonding to neighboring functionality *via* the indolic N-H bond⁶. As a result, Trp can be found enriched at centers of biochemical significance such as protein-protein interfaces, protein-lipid interfaces (2.9% abundance in membrane proteins^{7d}), as well as serving to maintain protein structural integrity through intraprotein non-covalent interactions⁷. Owing to Trp's electron-rich π -system, further enrichment of Trp can be observed in the redox proteome⁸.

We recently reported a method for Trp modification that circumvents Trp's modest nucleophilicity by instead utilizing Trp's propensity to engage in photo-induced electron trans-Specifically, we utilized fer $(PET)^9$. carbamoylpyridinium salt (1) that, upon irradiation with 302 nm light, couples PET with selective bond formation at Trp through a radical fragmentation/recombination process (Figure 1B). The reaction displayed good selectivity for Trp, as well as short reaction times, with the pyridinium reagent displaying high degrees of both thermal- and photo-stability. Following our report, Melchiorre^{10a}, Beier^{10b}, Paixão^{10c}, and Chiang^{10d} reported photochemical Trp modifications on small peptides using either Uv-A or visible light and organic solvents. Davis and Gouveurner also reported a three-step sequence to access functionalized Trp constructs using a difluoromethylation process featuring a ruthenium photocatalyst in a strongly reducing environment as part of the 24 hour long process^{10e}. Given the observed photo- and thermal stability of the 1 scaffold, coupled with its compatibility with pure aqueous environments and biological antioxidants such as glutathione (GSH), we considered that this scaffold could be readily adapted for use in chemoproteomic profiling. Additionally, the spatiotemporal control afforded by optical triggering enables control over aspects such as probe incubation time, allowing for sufficient time for cellular penetration and compartmentalization. Thus, chemoproteomic profiling using pyridinium salts to invoke the PET mechanistic manifold presents the opportunity to enrich an underexplored sub-section of the proteome that compliments current electrophilic strategies through enabling the discovery of new functionally critical Trp residues as well as sites of non-covalent interactions and biomolecular interfaces; in turn enabling their consideration as ligandable sites for drug discovery¹¹.

Results and Discussion

In seeking to develop a robust chemoproteomic profiling workflow using **1**, we noted the practical challenges of using filtered (to avoid wavelengths of <300 nm) Uv-B light as an irradiation source, as well as the potential for Uv-B light to induce photodegradation of labile proteins and unintended cellular stress¹². We have previously demonstrated that the mechanism of Trp labelling with **1** can be controlled in a reagent- and wavelength-dependent fashion by either invoking direct Trp photoexcitation ([Trp]*->1, Trp acts as a photoreductant) or by tuning the structure of **1** to enable exclu-

sive photoexcitation of 1 (Trp->[1]*, Trp acts as a reductive quencher); with the latter approach enabling modification of photolabile proteins. Using this observation, we rationalized that it should be possible to extend the π -conjugation of 1 to enable direct photoexcitation of 1 using the visible spectrum (Figure 1C). Concurrently, we recognized that structurally analogous cationic-aromatic photosensitizers, such as triaryl pyrylium salts, acridinium salts, and flavins are potent photooxidants that possess excited state redox potentials (S*/S• $E_{1/2}$) in excess of +1.8 eV¹³; which could possibly lead to a loss of chemoselectivity or photo-induced degradation of sensitive biological structure.

These considerations have led to the development of pyridinium scaffold 2, which possesses an electron-rich 6methoxynaphthyl ring appended at the 4-position to the cationic pyridinium moiety. This structural manifold creates a donor-acceptor relationship between the two aryl rings that both tempers the photo-oxidation potential of 2 and bathochromically shifts the absorbance of model probe 2a to beyond 450 nm (Figure 2A); in turn enabling optical activation with simple violet and blue LEDs. Irradiation of a degassed solution of 10 μM lysozyme in pH 6.9 NH₄OAc buffer, 300 μM glutathione (GSH) and 200 μM of 2a with a 427 nm LED (Kessil PR-160, 50W) in a Hepatochem Photoredoxbox photoreactor for 60 minutes resulted in the efficient labelling of lysozyme in >95% conversion and only low levels of glutathionylation observed (Figure 2B). MS-MS analysis confirms selectivity for Trp-62, analogous to our prior report^{9a}. Compared to our first generation probe designs (1),

2a demonstrates a marked enhancement in performance; efficiently labeling proteins at an order of magnitude lower concentration of both protein and probe whilst simultaneously affording optical triggering with visible light.

To better understand this enhanced kinetic profile, we studied the photophysical properties of 2a. Temporal control experiments verify the requirement of light to achieve labelling, and suppress chain-transfer driven mechanisms (Figure 2D). A Stern-Volmer plot of fluorescence quenching of 2a with small molecule Trp analog Nacetyltryptophamide (NATA) shows a measurable linear correlation, suggesting dynamic quenching of [2a]* with Trp (Figure 2C). 2a displays solvatochromatic properties that are associated with significant charge transfer in the photoexcited state, with TDDFT calculations supporting this excitation mode through a naphthyl->pyridinium charge transfer upon excitation from S0 to S1, with the biaryl motif adopting a coplanar orientation in S1 (Figure 2E). Owing to the irreversible peak reduction potential typical of the SET/fragmentation reactivity manifold of 2a and related scaffolds¹⁴, we computationally estimated the redox potential of 2a using the method of Nicewicz¹⁵. This approach estimates the $[2a^+]^*/2a^-$ excited state redox potential to be +1.330 eV; nearly 1 eV less oxidizing than tri-arylpyrylium catalysts^{13a}. Fluorescence lifetime measurements in 1,2dichloroethane and acetonitrile both show one-phase exponential decays that correlate to τ_1 = 4.1 ns and τ_1 = 3.3 ns respectively; suggesting a general decrease in lifetime as sol-

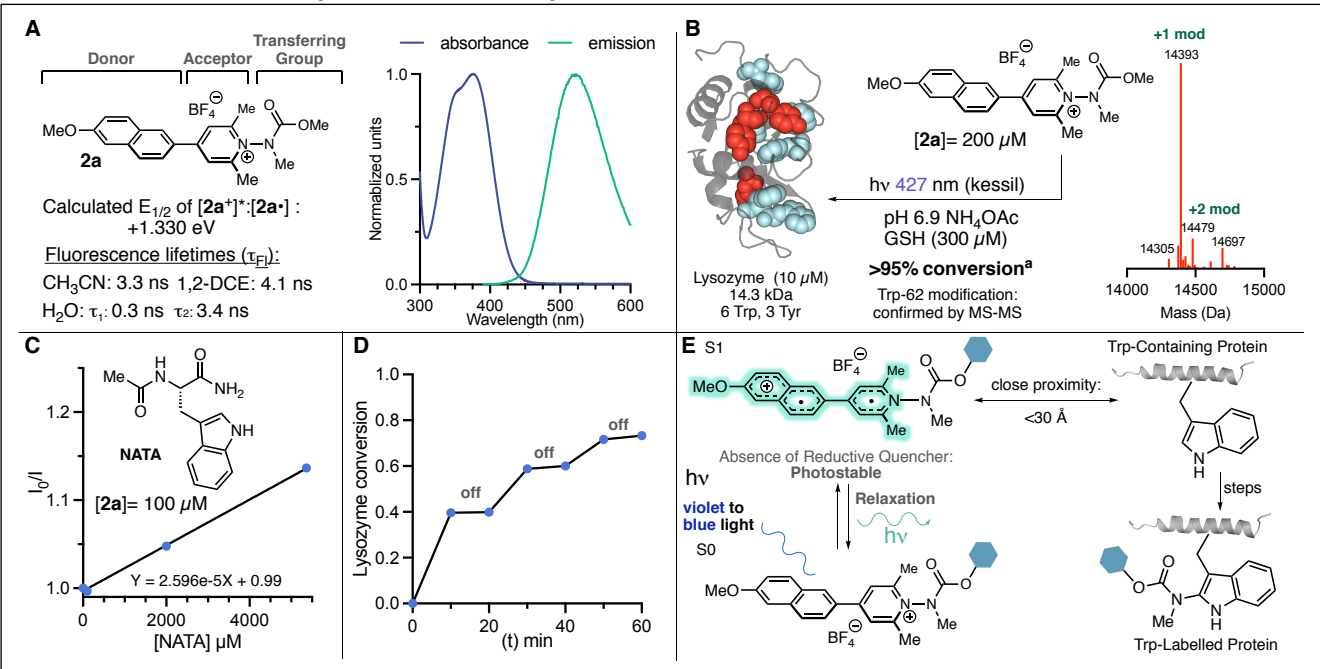


Figure 2. (A) Design, absorption/emission, fluorescence lifetimes, and calculated redox potentials of Trp probe 2a. Calculations were performed using B3LYP 6-31g(d) using an H_2O solvent cavity. (B) Labelling of lysozyme with 2a. Cyan residues=Trp, Red residues=Tyr. (C) Stern-Volmer plot of fluorescence quenching of 2a with NATA. (D) Establishment of temporal control with a lamp "on-off" experiment using identical conditions to those shown in Fig. 2B. (E) Mechanistic considerations for the requirement of proximity of $[2a]^*$ to the protein of interest. "Conversions are estimated by total ion count (TIC) and represent the average of two experiments.

vent polarity increases. However, two lifetimes are observed in water (τ_1 = 0.3 ns and τ_2 = 3.4 ns); with the second lifetime being of very weak intensity. Concurrently, the fluorescence intensity of 2a decreases with increasing solvent polarity (see supplementary figure S14). These data suggest that (1) the excited state of 2a is generally suppressed in aqueous systems compared to organic solvents and (2) $2a^*$ cannot defuse beyond 30 Å. When considered together, these observations lead us to propose that the observed selectivity for Trp modification by 2a is likely driven by a synergistic combination of a short-lived excited state that lacks the persistence to enable kinetically slower processes and protein-2a pre-complexation via hydrophobic effects, as well as a kinetic preference for Trp over other redox-active residues (Figure 2E).

Next, we sought to explore the scope of the labelling process. We therefore assembled a small battery of Trpcontaining peptides and proteins in which the Trp residues

are located in an array of differing environments (Figure 3A). Smaller peptides, such as Octreotide and Leuprolide are each labelled efficiently under violet LED irradiation conditions(see supplementary information). Exenatide • OAc, a 4.2 kDa polypeptide, possesses a single turn of the peptide backbone displays slightly diminished, but still efficient conversion (70%). Thioredoxin (Trx), an 11 kDa protein essential to disulfide formation, possesses two Trp residues, two Tyr residues and, in its reduced form, two Cys residues. Irradiation of Trx proceeded smoothly to afford Trp labelling at Trp-31. During the course of the labelling process, we noted disulfide bond formation. We next explored the labelling of β2-microglobulin (B2M), an 11.8 kDa structural component of the class I major histocompatibility complex, which features two Trp residues, one that is fully solventexposed and one that is largely buried, as well as 6 surface exposed Tyr residues. Irradiation of B2M with 2a for 30

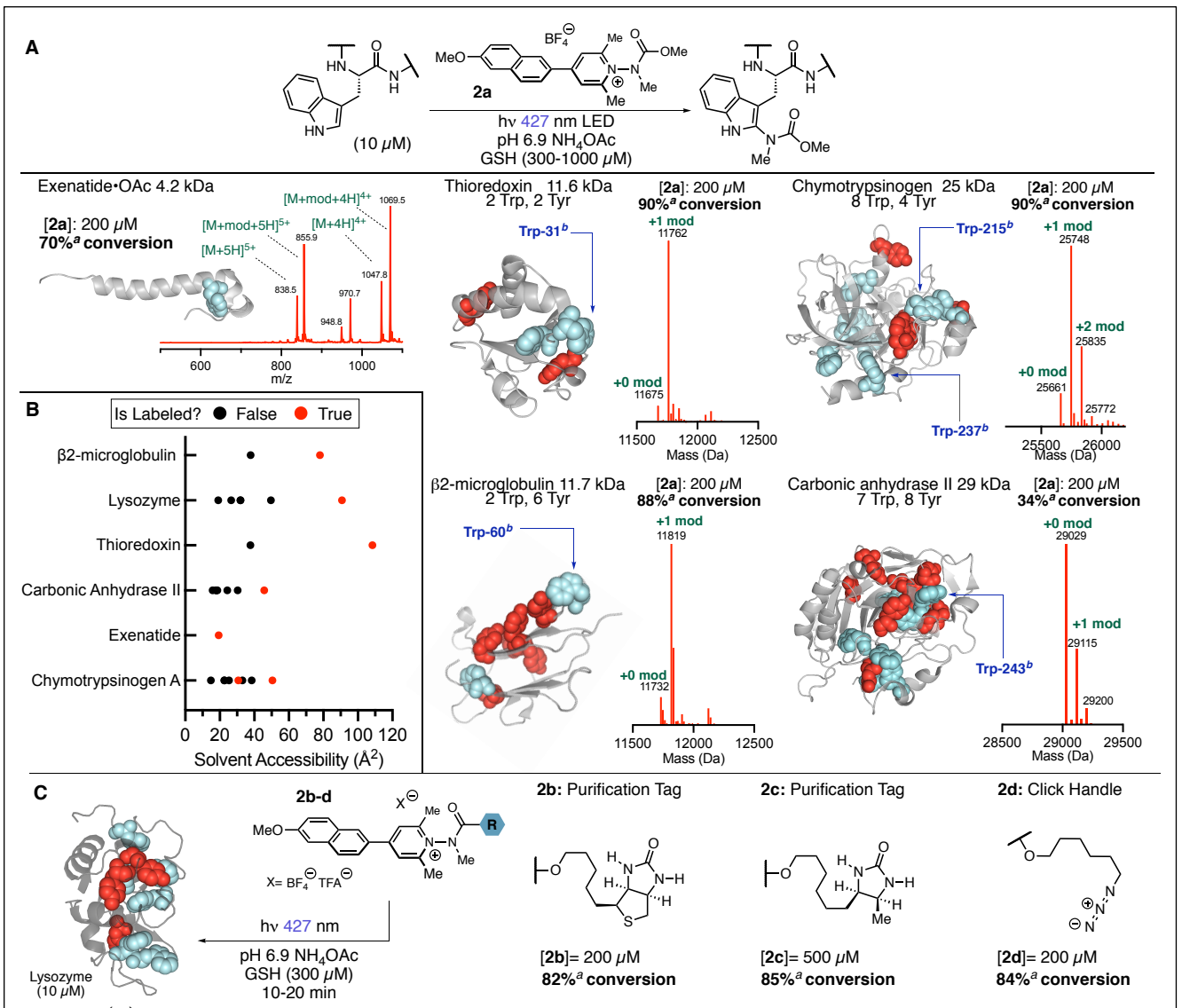


Figure 3. (**A**) Exploration of the labelling of Trp residues in various purified peptides and proteins using **2a**. Cyan residues=Trp, Red residues=Tyr. (**B**) Calculated solvent accessibilities for all modified and unmodified Trp residues except that of Octreotide are highlighted in the boxplot. (**C**) Transferring group scope using the **2** scaffold. ^aConversions estimated by (TIC) and represent the average of two experiments. ^bModification sites confirmed by MS-MS.

minutes led to almost exclusive mono-labelling at solvent exposed Trp-60 in 88% conversion. Chymotrypsinogen A, a 25 kDa protein, possesses 8 Trp residues and 4 Tyr residues, efficiently labels in 90% conversion, with a 21:8:1 ratio of mono:di:tri labelling. Digestion/MS-MS elucidated Trp-215 and Trp-237 to be the detectable locations of labelling in this protein. Finally, we investigated the labelling of bovine carbonic anhydrase II (CAII). CAII possesses 7 Trp residues, most of which are either completely buried or have very limited solvent exposure. As a result, CAII displayed much lower levels of conversion (34%), with Trp-243 being the identifiable site of modification. Taken together, these results establish the selectivity of 2a for Trp over an array of environments. Plotting the solvent accessibility of each Trp residue in peptides and proteins weighing greater than 4 kDa and comparing against modification sites indicates that 2a typically selects for the most solvent accessible residue when multiple choices are present (Figure 3B). In examples where there is a single Trp residue that is poorly exposed, such as Exenatide, modification can still be observed, albeit with reduced conversion. It also suggests that 2a is sensitive to local steric environments, not just with respect to surface exposure, but also to adequate surface exposure of the indolic C2 position as this position is the preferred site of carbamylation. We also note that these labelling reactions generally demonstrate clean reaction profiles, indicating that 2a does not cause significant levels of photodegradation.

We then turned our attention to the use of $\mathbf{2}$ to transfer useful functionality to Trp residues (Figure 3C). In that regard, we found that affinity tags such as biotin $(\mathbf{2b})$ are

efficiently transferred to lysozyme in 82% conversion. Notably, protein labelling with 2b proceeded at a much faster rate than with 2a; with complete reactivity observed in less than 10 minutes, as opposed to 60 minutes with 2a. Fluorescence lifetime experiments show that **2b** has a shorter τ_2 (τ_1 = 0.5 ns and τ_2 = 2.8 ns) than **2a** whilst comparison of emission spectra reveal that 2b has a higher fluorescence quantum yield $(\Phi_{\rm Fl})$ than **2a** (relative $\Phi_{\rm Fl}$ **2b**:**2a** = 3.3) (Figure S14D); suggesting a correlation between Φ_{FI} and kinetics. Desthiobiotinylation with 2c also proceeded with an enhanced rate, but required a larger excess of probe ($[2c]=500 \mu M \text{ vs.} [2b]=200$ μM) in order to observe comparable labelling efficiency. The difference in reactivity between these two structurally similar probes can, in part, be attributed to subtle differences in water solubility, but the origins of this difference require further investigation. Azide probe 2d also showed enhance rates compared to 2a, and was smoothly transferred to lysozyme in 84% conversion with just 20 minutes of irradiation time.

Having demonstrated efficient reactivity and selectivity towards Trp modification in purified peptide/protein systems, we next sought to assess the capabilities of $\bf 2$ in chemoproteomic profiling. We assembled three biotinylated Trp probes, $\bf 2b$, as well as probes $\bf 1a$ and $\bf 1b$, which featured our previously reported pyridinium designs against proteome profiling of HEK293T lysates. Lysates (5 mg/ml) were incubated with the desired probe at varying concentrations (0-100 μ M) for 60 minutes and subsequently irradiated for 20 minutes with the following light sources: unfiltered 302 nm

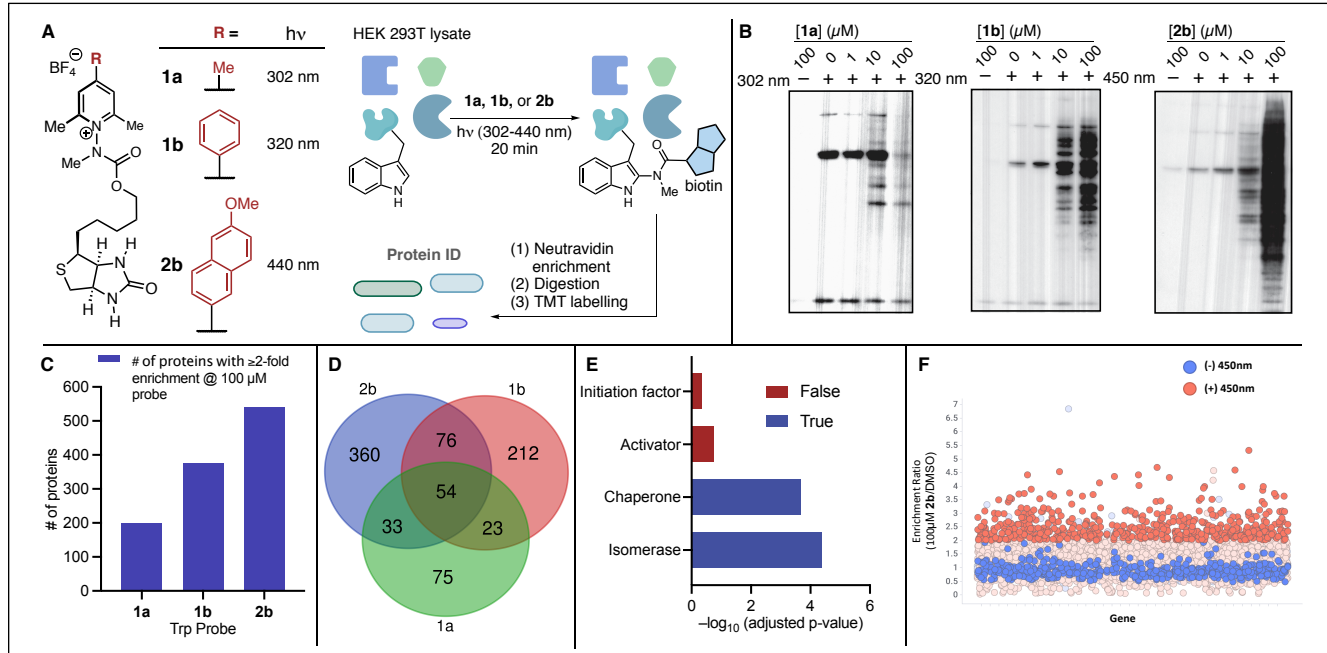


Figure 4. (A) Evaluation of three Trp probe designs against HEK293T lysates. All experiments were performed in duplicate. (B) Post-enrichment elution profiles of 1a, 1b, and 2b at 0-100 μM probe and at 100 μM probe in the absence of light. (C) Number of proteins identified at 100 μM of each probe. (D) Venn diagram comparing overlap of proteome coverage by each probe. (E) Classes of proteins showing significant enrichment relative to all detected proteins with $100 \, \mu M \, 2b$. – $Log_{10} \, p$ -values are shown to clearly highlight enrichment. (F) Light dependence of protein-level enrichment with 2b.

light for 1a, filtered 320 nm light for 1b, and 440 nm light for **2b** (Figure 4A). Biotinylated proteins were then enriched *via* neutravidin and washed to remove nonspecifically bound proteins. The enriched proteins were eluted and subsequently digested in solution followed by Tandem Mass Tag (TMT) labelling, and protein identification and quantitation by LC/MS-MS. Western blot analysis using streptavidin-HRP of elution profiles for probes 1a, 1b and 2b before digestion indicated that each probe displays concentration and optically dependent proteome labelling profiles. Notably, we observed a loss of signal with trimethyl probe 1a at the highest assayed conditions, 100 µM (Figure 4B). It is possible that this loss of signal correlates to photodegradation associated with the generation of an excess of high energy photoexcited states of 1a, which could originate from the lower wavelength light emitted by the unfiltered 302 nm light source. Both probes 1b and 2b showed expected doseresponse profiles. Following enrichment and digestion, LC/MS-MS analysis led to the identification (from ≥ 2 unique peptides) of 185 proteins with 1a, 365 proteins with

1b, and 523 proteins with **2b** that showed \geq 2-fold enrichment at 100 µM concentration vs. DMSO (Figure 4C). A comparison of proteome coverage of each probe reveals 2b has the highest percentage (69%) of unique enriched proteins (Figure 4D). In order to understand what types of protein functions are enriched with 2b, an enrichment analysis of proteins displaying ≥ 2 -fold enrichment with **2b** versus all proteins detected in the experiment was performed (Figure 4E). This analysis indicated that chaperone and isomerase proteins an especially high degree of enrichment against the background. A complete enrichment analysis and list of enriched proteins organized by class are available in supplementary information figures S23 and S24. Analysis of enrichment profiles for identified proteins with probe 2b in both the presence and absence of photoirradiation clearly illustrates both photo-induced reactivity of this probe as well as its thermal inertness in the absence of light (Figure 4F). During the completion of our studies, a pre-print from Hacker used an alkynylated derivative of la as part of an elegant study of profiling S. aureus and MDA-MB-231 cell ly-

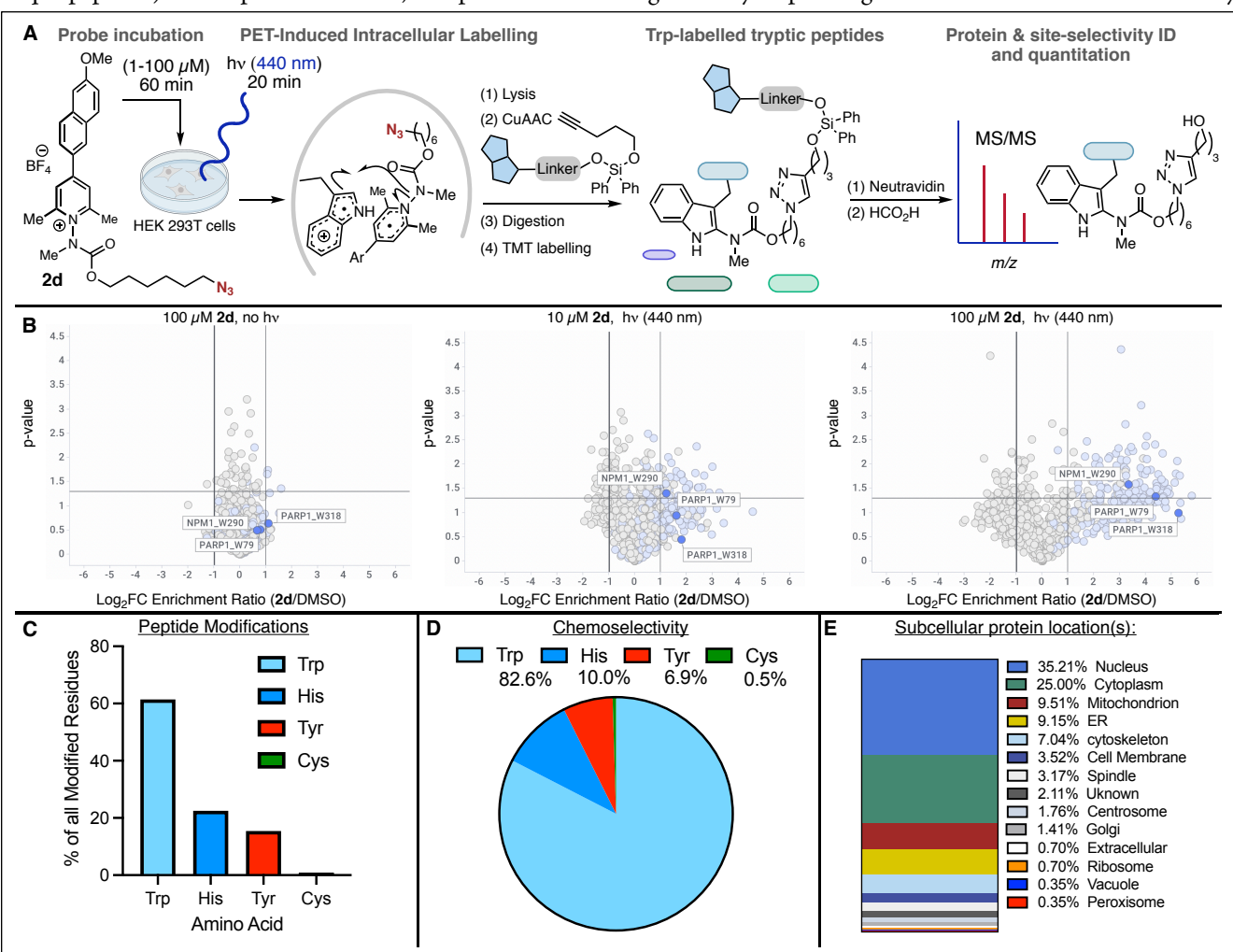


Figure 5. (A) Workflow for peptide level enrichment of Trp in HEK293T cells using bifunctional probe 2d. (B) Volcano plots showing light-dependent and dose-responsive enrichment of the tryptophan-ome from 10-100 μ M Trp. Average of two experiments. Light blue dots indicate enriched peptides harboring Trp modifications. Dark blue dots indicate labelled Trp in NPM1 and PARP1. (C) Detected residue modifications by percentage. (D) Chemoselectivity based upon amino acid relative frequency. (E) Subcellular localization of Trp-modified proteins.

sates with multiple bioconjugation probes¹⁶.

Next, we sought to label and identify Trp modifications through intracellular PET labelling in cultured HEK293T cells. Owing to the superior performance of clickable azide probe 2d over desthiobiotin probe 2c in labelling purified proteins, we opted for use of 2d in these studies. Thus, live HEK293T cell cultures were incubated with 1-100 μM concentrations of 2d for 60 minutes at 37°C, followed by photoirradiation with 440 nm light for 20 minutes at 4°C. Lysates were then generated, followed by CuAAC to install an acid-cleavable alkyne-DADPS-biotin (DADPS=dialkoxydiphenyl silane) affinity tag17, digestion, TMT labelling, and recombination of TMT-labelled samples. Enrichment of this mixture with neutravidin, followed by release of captured tryptic peptides with 10% formic acid yielded peptides harboring covalent modifications that were then identified and quantified by LC/MS-MS (Figure 5A). As evidenced in Figure 5B, 2d enables light and dose-dependent enrichment of Trp-modified peptides, with measurable 2-fold enrichment at low (10 µM) concentrations of probe. We also noted that 2d displays robust thermal stability under whole cell culture conditions and the lack of peptide enrichment without 440 nm photoirradiation demonstrates spatiotemporal control. At 100 µM of 2d, the above workflow enabled the detection of 290 Trp-modified peptide fragments showing dose-response behavior that correspond to 209 unique proteins (blue dots). Selectivity for Trp modification is maintained in situ and demonstrates the ability to enrich the tryptophan-ome directly from whole cell culture. Analysis of the chemoselectivity profile of **2d** reveals 221 unique peptides harboring a Trp modification, with minor levels of modifications observed at His, Tyr, and Cys (Figure 5C). When the relative amino acid frequency of these residues in human proteins is taken into account, **2d** displays 82% selectivity for Trp (Figure 5D).

Proteins with detected Trp modifications were analyzed against the UniProt database for subcellular localization profiles (Figure 5E). A majority of identified proteins were found to have at least partial localization within the nucleus and the cytoplasm, followed by the mitochondria and endoplasmic reticulum. In addition to evidencing that **2d** readily crosses the plasma membrane, this analysis also indicates that the net positive charge of **2d** does not restrict Trp modification to mitochondrial proteins. Rather, **2d** is able to penetrate a wide variety of important subcellular regions and can enrich the tryptophan-ome in a wide array of areas.

Chemoproteomic profiling with **2d** enabled dose-dependent enrichment of functionally critical Trp residues (Figure 6A). For example, chemoproteomic Trp profiling with **2d** enabled *in situ* labelling of Trp290 of the nuclear protein NPM1. NPM1 is a protein involved in a wide array of cellular functions revolving around genomic homeostasis¹⁸. In line with previous solvent accessibility observations, Trp288 has a lower calculated solvent accessibility score compared to Trp290 and was not labelled in our studies. Mutation of Trp290 and Trp288, which are commonly

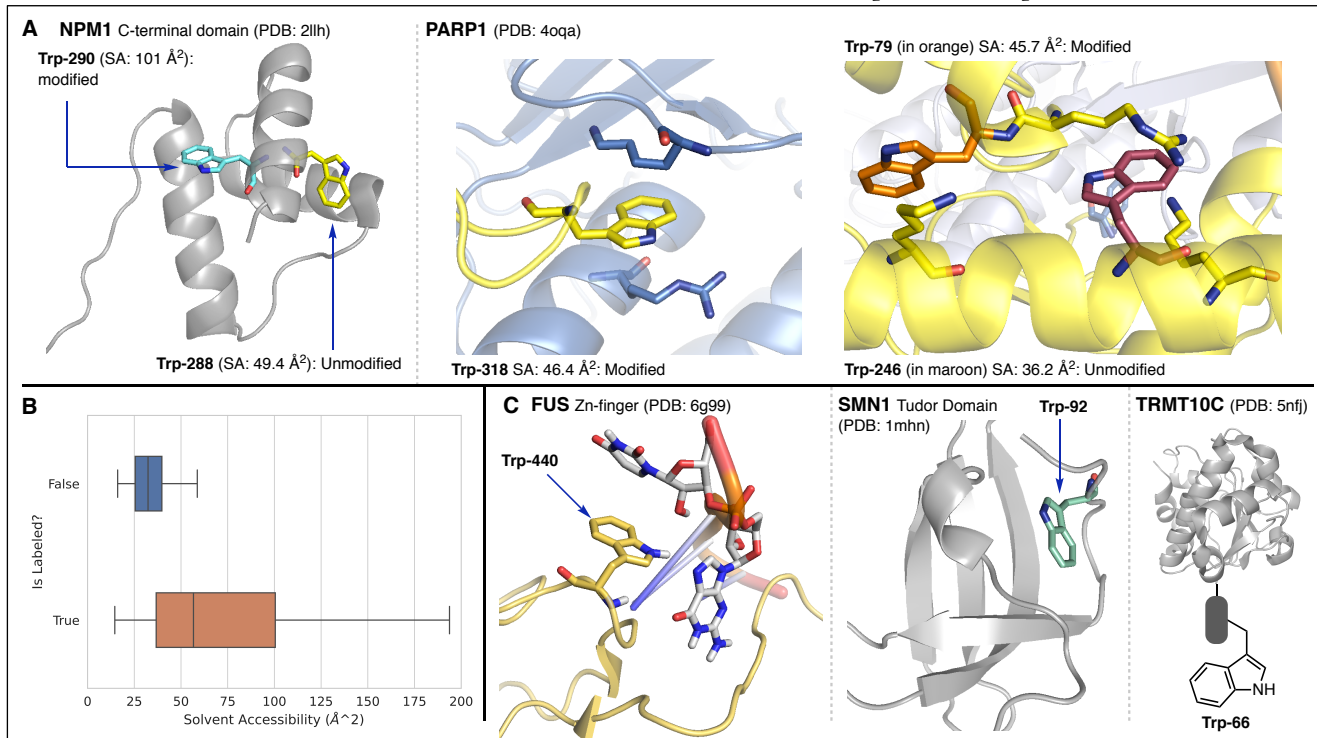


Figure 6. (**A**) Modification of functionally critical Trp residue in nuclear proteins NPM1 (Trp-290) and PARP1 (Trp-79 and Trp-318). Residues engaging in non-covalent interactions with both Trp residues PARP1 are highlighted. Functionally critical Trp-246, which has lower solvent accessibility and was not modified, is also highlighted. SA=solvent accessibility. (**B**) Comparison of solvent accessibility in modified and unmodified Trp residues of proteins identified *in situ* with **2d**. (**C**) Modified Trp residues on proteins associated with various disease states.

found in cases of acute myeloid leukemia, results in misfolding of the C-terminal domain and translocation of the protein to the cytosol^{18b}. We also observed the modification and dose-dependent enrichment of Trp79 and Trp318 in PARP1; an essential protein in DNA damage detection and repair, gene transcription regulation, and cell death signaling¹⁹. Trp79 and Trp318 participate in non-covalent interactions at the interface between various domains of PARP1, and mutation of these residues resulted in either partial (Trp79) or complete (Trp318) loss of catalytic activity^{19c,d}.

In both of these examples, we noted the same Trp modification selectivity trend that we observed in our studies on model proteins from Figure 3; namely that $\bf 2$ selects for Trp residues with the greatest solvent accessibility when multiple Trp residues are present. We then expanded upon these observations by conducting a survey of all Trp residues found on the proteins identified from our *in situ* studies (for which structural data is available) for solvent accessibility (Figure 6B). Given a maximum theoretical surface exposure of 264 Ų, modified Trp residues were found to be 21% accessible (average accessible area = 56 Ų) whilst unmodified Trp residues were only 12% accessible (average accessible area = 32 Ų); a statistically significant difference²0. This data further reinforces a preference for $\bf 2$ to label Trp residues with enhanced surface exposure.

Whilst we were able to enrich Trp residues with known function, cross-referencing identified proteins against the Drugbank database revealed that a majority of identified proteins (75%) do not have Drugbank entries (Figure S25). A search of modified Trp residues for residue/region specific annotation in the UniProt database indicated that a large majority (92%) of modified residues have no functional annotation assigned to them (Figure S25). The most common functional annotations found involved Trp residues located in trans-membrane regions of the parent protein (6%), whilst 2% of Trp residues had established function based upon mutagenesis experiments. This very low percentage of residue annotation contrasts to other chemoproteomic profiling workflows that target more highly studied residues^{2a-f} and suggests potential for this method to enable the discovery of functionally important Trp residues.

To illustrate this, we have highlighted three proteins that have both been implicated in various disease states and harbor Trp residues that were modified with **2d** in Figure 6C as Trp residues of potential interest for further study. We observed modification of Trp440 in nucleotide-binding protein FUS. FUS has been implicated in numerous neurodegenerative diseases²¹, including ALS, and a recent NMR structure shows Trp440 participating in the non-covalent interactions with nucleobases^{21b}. The observed reactivity of Trp440, coupled with its participation in RNA binding, suggests this residue plays an active role in protein function. **2d** also modifies Trp92 in the tudor domain of SMN1. It was shown that mutation of this residue occurs in some instances of spinal

muscular atrophy and is active in the disease state by inhibiting SMN1-protein interactions²². These observations, combined with the reactivity of this Trp residue towards **2d**, highlight it as a candidate for further systematic study and also highlights the potential importance of Trp residues in the function of Tudor domains found in other proteins. **2d** also labels Trp66 in mitochondrial protein TRM10C, a protein responsible for mitochondrial RNA processing²³. Loss of protein function leads to defects in mitochondrial protein synthesis and aerobic respiration. These proteins highlight the ability of **2d** to modify disease-associated proteins across multiple cellular locations.

Finally, we validated the identification of NPM1 and PARP1 as enriched targets with 2d (Figure 7A). HEK293T cells were treated with varying concentrations of 2d both in the presence and absence of blue light, followed by protein level enrichment. The resultant enriched protein mixtures were then analyzed via western analysis and found to contain both proteins when cultures were irradiated in the presence of 2d. No enrichment of these proteins was found in either the absence of probe or the absence of light. We further validated NPM1 enrichment by directly labelling an NPM1 C-terminal construct (residues 240-294), 3, which possesses both residues in NPM1 (Figure 7B). Briefly, 3 was irradiated at 440 nm with probe 2b for 15 minutes. Western analysis confirmed photo-dependent labelling of the construct. We also observed temperature dependence of labelling, wherein labelling at 50 °C leads to a higher level of labelling. It is likely that 3 is tightly folded at room temperature under the labelling conditions used, with elevated temperatures causing partial relaxation of the structure, in turn leading to enhanced labeling.

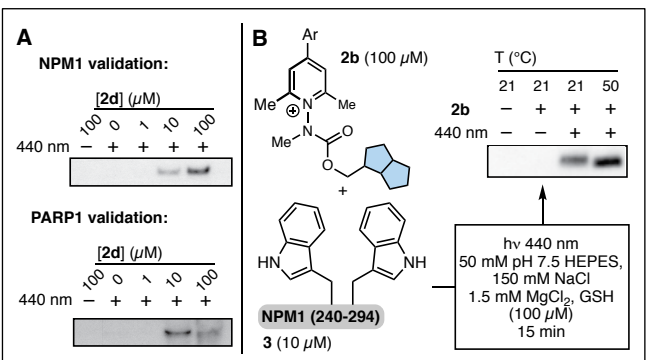


Figure 7. (**A**) Validation of the identification of NPM1 and PARP1 *via* western analysis of post-protein level enrichment profiles of HEK293T cells labelled with **2d**. (**B**) Labelling of a recombinant NPM1 C-terminal construct with **2b**.

Conclusions

In summary, we have developed a donor-acceptor pyridinium salt scaffold (2) that enables PET-driven Trp modification in proteins using visible light. We demonstrate that 2 labels purified Trp-containing proteins at an order of magnitude more dilute conditions over our previous design whilst

maintaining good conversions and selectivity. The carbamate transferring group can be used to install functional handles useful for chemoproteomics and general bioconjugation strategies on to proteins. Photophysical analyses and DFT calculations provide insight into the electronic structure and photochemical behaviors of **2** in the context of observed chemical outcomes; providing mechanistic insight for future probe designs. We also demonstrated that **2** is suited for chemoproteomic profiling; enabling enrichment of the tryptophan-ome from both lysates and live cell culture. We anticipate that **2** can be readily incorporated into chemoproteomic workflows that both probe for ligandable sites that do not possess traditional nucleophilic residues as well as to explore the basic *in situ* chemical behavior of Trp.

ASSOCIATED CONTENT

Supporting information includes experimental procedures for probe synthesis, protein modification experiments, photophysical studies, chemoproteomic profiling and computational analysis. A second spreadsheet contains chemoproteomic profiling data tables.

The Supporting Information is available free of charge on the ACS Publications website.

AUTHOR INFORMATION

Corresponding Author

*mtaylo45@uwyo.edu

ORCID

Michael T. Taylor: 0000-0002-7655-7222

Nicholas J. Kuehl: 0000-0003-3640-8596

Akash M. Sarkar: 0000-0002-0277-6916 Markus Schirle: 0000-0003-4933-2623

Author Contributions

‡These authors contributed equally.

Notes

The authors declare the following competing financial interest(s): FJG, DTB, GEM, TRB, CHH MDJ, MS are employees of Novartis Institutes for BioMedical Research.

ACKNOWLEDGMENT

We acknowledge SBC **COBRE** program (5P20GM121310-02) for support. Additionally, this material is based upon work supported by the Chemistry of Life Processes Program in the National Science Foundation Division of Chemistry under Grant CHE-2048201. acknowledges the Wyoming Research Scholars Program and Wyoming NASA space grant consortium (NNX15AI08H) for student fellowships. Partial instrumentation support was provided by the NSF grant CHE- 1429615. We thank Prof. Caleb Hill for assistance with acquiring cyclic voltammetry data for **2a**.

REFERENCES

- (1)(a) Niphakis, M.J.; Cravatt, B.F. Enzyme Inhibitor Discovery by Activity-Based Protein Profiling. Annu. Rev. Biochem. 2014, 83, 341–77. (b) Cravatt, B.F.; Wright, A.T.; Kozarich, J.W. Activity-Based Protein Profiling: From Enzyme Chemistry to Proteomic Chemistry. Annu Rev Biochem. 2008, 77, 383–414. (c) Heal, W.P.; Dang. T.H.T.; Tate, E.W. Activity-based probes: discovering new biology and new drug targets. Chem Soc Rev. 2011, 40, 246–57. (d) Chan, W.C.; Sharifzadeh, S.; Buhrlage, S.J.; Marto, J.A. Chemoproteomic methods for covalent drug discovery. Chem. Soc. Rev. 2021, 50, 8361-8381. (e) Spradlin, J.N.; Zhang, E.; Nomura, D.K. Reimagining Druggability Using Chemoproteomic Platforms. Acc. Chem. Res. 2021, 54, 1801-1813.
- (2) For reviews summarizing cysteine profiling: (a) Maurais, A.J.; Weerapana, E. Reactive-cysteine profiling for drug discovery. Curr. Op. Chem. Biol. 2019, 50, 29-36. (b) Backus, K.M.; Applications of Reactive Cysteine Profiling. Curr. Top. Microbiol. Immunol. 2019, 420, 375-417. (c) Guan, I.; Williams, K.; Pan, J.; Liu, X. New Cysteine Covalent Modification Strategies Enable Advancement of Proteome-wide Selectivity of Kinase Modulators. Asian J. Org. Chem. 2021, 10, 949-963. For examples of lysine profiling: (d) Hacker, S.M.; Backus, K.M.; Lazear, M.R.; Forli, S.; Correia, B.E.; Cravatt, B.F. Global profiling of lysine reactivity and ligandability in the human proteome. Nature Chemistry. 2017, 9, 1181-1190. (e) Shannon, D.A.; Banerjee, R.; Webster, E.R.; Bak, D.W.; Wang, C.; Weerapana, E. Investigating the Proteome Reactivity and Selectivity of Aryl Halides. J. Am. Chem. Soc. 2014, 136, 3330-3333. For examples targeting N-, O- and S-nucleophiles: (f) Ward, C.C.; Kleinman, J.I.; Nomura, D.K. NHS-Esters As Versatile Reactivity-Based Probes for Mapping Proteome-Wide Ligandable Hotspots. ACS Chem. Biol. 2017, 12, 1478-1483. For examples of Tyrosine profiling: (g) Brulet, J.W.; Borne, A.L.; Yuan, K.; Libby, A.H.; Hsu, K-L. Liganding Functional Tyrosine Sites on Proteins Using Sulfur-Triazole Exchange Chemistry. J. Am. Chem. Soc. 2020, 142, 18, 8270-8280. (h) Sun, F.; Suttapitugsakul, S.; Wu, R. An Azo Coupling-Based Chemoproteomic Approach to Systematically Profile the Tyrosine Reactivity in the Human Proteome. Anal. Chem. 2021, 93, 10334-10342.
- For Carboxylic acid profiling: (i) Bach, K.; Beerkens, B.L.H.; Zanon, P.R.A.; Hacker, S.M. Light-Activatable, 2,5-Disubstituted Tetrazoles for the Proteome-wide Profiling of Aspartates and Glutamates in Living Bacteria. *ACS. Cent. Sci.* **2020**, 6, 546-554. (j) Ma, N.; Hu, J.; Zhang, Z-M.; Liu, W.; Huang, M.; Fan. Y.; Yin, X.; Wang, J.; Ding, K.; Ye, W.; Li, Z. *2H*-Azirine-Based Reagents for Chemoselective Bioconjugation Carboxyl Residues Inside Live Cells. *J. Am. Chem. Soc.* **2020**, 142, 6051-6059. For Methionine profiling: (k) Lin, S.; Yang, X.; Jia, S.; Weeks, A.M.; Hornsby, M.; Lee, P.S.; Nichiporuk, R.V.; Iavarone, A.T.; Wells, J.A.; Toste, F.D.; Chang, C.J. Redox-based reagents for chemoselective methionine bioconjugation. *Science.* **2017**, 355, 597-602.
- (3) Lakhdar, S.; Westermaier, M.; Terrier, R.; Boubaker, T.; Ofial, A.R.; Mayr, H. Nucleophilic Reactivites of Indoles. *J. Org. Chem.* **2006**, 71, 24, 9088-9095.
- (4) (a) Scoffone, E.; Fontana, A.; Rocchi, R. Sulfenyl halides as Modifying Reagents for Polypeptides and Protein I. Modification of Tryptophan Residues. *Biochemistry.* **1968**, 7, 971-979. (b) Kuyama, H.; Watanabe, M.; Toda, C.; Ando, E.; Tanaka, K.; Nishimura, O. An approach to quantitative proteome analysis by labeling tryptophan residues. *Rapid Commun. Mass Spectrom.* **2003**, 17, 1642-1650. (c) Antos, J.M.; McFarland, J.M.; Ivarone, A.T.; Francis, M.B. Chemoselective Tryptophan Labeling with Rhodium Carbenoids at Mild pH. *J. Am. Chem. Soc.* **2009**, 131, 6301-6308. (d) Ball, Z.T. Designing Enzyme-like Catalysts: A Rhodium(II) Metallopeptide Case Study. *Acc. Chem. Res.* **2013**. 46, 560-570. (e) Seki, Y.; Ishiyama, T.; Sasaki, D.; Abe, J.; Sohma, Y.; Oisaka, K.; Kanai, M. Transition Metal-Free Tryptophan-Selective Bioconjugation of Proteins. *J. Am. Chem. Soc.* **2016**, 138, 10798-10801. (f) Wang, W.; Lorion, M.M.; Shah, J.; Kapdi, A.R.; Ackermann, L. Late-Stage Peptide Diversification by Position-Selective C-

- H activation. *Angew. Chem. Int. Ed.* **2018**, 57, 2-20. (g) Petersen, J.; Christensen, K.E.; Nielsen, M.T.; Mortensen, K.T.; Komnatnyy, V.V.; Nielsen, T.E.; Qyortrup, K. Oxidative Modification of Tryptophan-Containing Peptides. *ACS. Comb. Sci.* **2018**, 20, 344-349. (h) Foettinger, A.; Leitner, A.; Lindner, W. Selective Enrichment of Trytophan-Containing Peptides from Protein Digests Employing a Reversible Derivatization with Malondialdehyde and Solid-Phase Capture on Hydrazide Beads. *J. Proteome Res.* **2007**, 6, 3827-3834. (i) Yu, Y.; Zhang, L.K; Buevich, A.V.; Li, G.; Tang, H.; Vachal, P.; Colletti, S.L.; Shi, Z.C. Chemoselective peptide Modification via Photocataliyic Tryptophan β-position Conjugation. *J. Am. Chem. Soc.* **2018**, 140, 6797-6800.
- (5) (a) Tsai, C-J.; Lin, S.L.; Wolfson, H.J.; Nussinov, R. Studies of protein-protein interfaces: A statistical analysis of the hydrophobic effect. *Protein Sci.* **1997**, *6*, 53-64. (b) Ma, B.; Elkayam, T.; Wolfson, H.; Nussinov, R. Protein-protein interactions: Structurally conserved residues distinguish between binding sites and exposed protein surfaces. *Proc. Natl. Acad. Sci.* **2003**, 100, 5772-5777.
- (6) (a) Ma, J.C.; Dougherty, D.A. The Cation- π Interaction. *Chem. Rev.* **1997**, 97, 1303-1324. (b) Mecozzi, S.; West Jr., A.P.; Dougherty, D.A. Cation-pi interactions in aromatics of biological and medicinal interest: electrostatic potential surfaces as a useful qualitative guide. *Proc. Natl. Acad. Sci. USA.* **1996**, 93, 10566–10571. (c) Gallivan, J.P.; Dougherty, D.A. Cation- π interactions in structural biology. *Procl. Natl. Acad. Sci.* **1999**, 17, 9459-9464. (d) Steiner, T.; Koellner, G. Hydrogen Bonds with π -Acceptors in Proteins: Frequencies and Role in Stabilizing Local 3D Structures. *J. Mol. Bio.* **2001**, 305, 535-557. (e) Bissantz, C.; Kuhn, B.; Stahl, M. A Medicinal Chemist's Guide to Molecular Interactions. *J. Med. Chem.* **2010**, 53, 5061-5084.
- (7) (a) Ma, B.; Nussinov, R. Trp/Met/Phe Hot Spots in Protein-Protein Interactions: Potential Targets in Drug Discovery. *Curr. Top. Med. Chem.* **2007**, 7, 999-1005. (b) de Jesus, A.J.; Allen, T.W. The role of tryptophan side chains in membrane protein anchoring and hydrophobic mismatch. *BBA-Biomembranes.* **2013**, 1828, 864-876. (c) Liu, W.; Caffrey, M. Interactions of Tryptophan, Tryptophan Peptides, and Tryptophan Alkyl Ester at Curved membrane Interfaces. *Biochemistry.* **2006**, 45, 11713-11726. (d) Barik, S. The Uniqueness of Tryptophan in Biology: Properties, Metabolism, Interactions and Localization in Proteins. *Int. J. Mol. Sci.* **2020**, 21, 8776-8797.
- (8) Winkler, J.R.; Gray, H.B. Could tyrosine and tryptophan serve multiple roles in biological redox processes? *Phil. Trans. R. Soc. A.* **2015**, 373, 20140178.
- (9) (a) Tower, S.J.; Hetcher, W.J.; Myers, T.E.; Kuehl, N.J.; Taylor, M.T. Selective Modification of Tryptophan Residues in Peptides and Proteins Using a Biomimetic Electron Transfer Process. *J. Am. Chem. Soc.* **2020**, 142, 9112-9118. (b) Orellana, N.V.; Taylor, M.T. Targeting Trp for Tagging through Photoinduced Electron Transfer. *Synlett.* **2021**, DOI: 10.1055/a-1479-6366
- (10) (a) Laroche, B.; Tang, X.; Archer, G.; Di Sanza, R.D.; Melchiorre, P. Photochemical Chemoselective Alkylation of Tryptophan-Containing Peptides. *Org. Lett.* **2021**, 23, 285-289. (b) Rahimidashaghoul, K.; Klimánková, I.; Hubálek, M.; Matoušek, V.; Filgas, J.; Slavíček, P.; Slanina, T.; Beier, P. Visible-Light-Driven Fluoroalkyaltion of Tryptophan Residues in Peptides. *ChemPhotoChem.* **2021**, 5, 43-50. (c) Lima, R.N.; Delgado, J.A.; Bernardi, D.I.; Berlinck, R.G.S.; Kaplaneris, N.; Ackermann, L.; Paixão, M.W. Post-synthetic functionalization of tryptophan protected peptide sequences through indole (C-2) photocatalytic alkylation. *Chem. Commun.* **2021**, 57, 5758-5761. (d) Weng, Y.; Ding, B.; Liu, Y.; Song, C.; Chan, L-Y.; Chiang, C-W. Late-Stage Photoredox C-H Amidation of *N-Unprotected Indole Derivatives: Access to N-(Indol-2-yl)amides. Org. Lett.* **2021**, 23, 2710-2714. (e) Imiolek, M.; Isenegger, P.G.; Ng, W-L.; Khan, A.; Davis, B.G. Residue-Selective Protein C-Formylation via Sequential Difluoroalkylation-Hydrolysis. *ACS. Cent. Sci.* **2021**, 7, 145-155.
- (11) Scott, D.E.; Bayley, A.R.; Abell, C.; Skidmore, J. Small molecules, big targets: drug discovery faces the protein-protein interaction challenge. *Nat. Rev. Drug Discov.* **2016**, 15, 533-550.
- (12) (a) Pattison, D.I.; Davis, M.J. Actions of ultraviolet light on cellular structure. Cancer: Cell Structures, Carconigens and Genmoic Instability.

- **2006**, 131-157. (b) Pattison, D.I.; Rahmanto, A.S.; Davies, M.J. Photo-oxidation of proteins. *Photochem. Photobiol. Sci.* **2012**, 11, 38-53.
- (13) (a) Romero, N.A.; Nicewicz, D.A. Organic Photoredox Catalysis. *Chem. Rev.* **2016**, 116, 10075-10166. (b) Dongare, P.; Mackenzie, I.; Wang, D.; Nicewicz, D.A.; Meyer, T.J. *Proc. Natl. Acad. Sci.* **2017**, 114, 9279-9283.
- (14) He, F-S.; Ye, S.; Wu, J. Recent Advances in Pyridinium Salts as radical Reservoirs in organic Synthesis. *ACS Catal.* **2019**, *9*, 8943-8960.
- (15) Roth, H.G.; Romero, N.A.; Nicewicz, D.A. Experimental and Calculated Electrochemical Potentials of Common Organic Molecules for Applications to Single-Electron Redox Chemistry. *Synlett.* **2016**, 27, 714-723.
- (16) Zanon, P.R.A.; Yu, F.; Musacchio, P.; Lewald, L; Zollo, M.; Krauskopf, Mrdović, D.; Raunft, P.; Maher, T.E.; Cigler, M.; Chang, C.; Lang, K.; Toste, F.D.; Nesvizhskii, A.I.; Hacker, S.M. Profiling the proteome-wide selectivity of diverse electrophiles. *ChemRxiv*. 2021. This content is a preprint and has not been peer-reviewed. DOI: 10.33774/chemrxiv-2021-w7rss-v2.
- (17) Szychowski, J.; Mahdavi, A.; Hodas, J. J. L.; Bagert, J. D.; Ngo, J. T.; Landgraf, P.; Dieterich, D. C.; Schuman, E. M.; Tirrell, D. A. Cleavable Biotin Probes for Labeling of Biomolecules via Azide– Alkyne Cycloaddition. *J. Am. Chem. Soc.* **2010**, 132, 18351–18360.
- (18)(a) Box, J.K.; Paquet, N.; Adams, M.N.; Boucher, D.; Bolderson, E.; O'Byrne, K.J.; Richard, D.J. Nucleophosmin: from structure and function to disease development. *BMC Molecular Biol.* **2016**, 17, 19. (b) Grummitt, C.G.; Townsley, F.M.; Johnson, C.M.; Warren, A.J.; Bycroft, M. Structural Consequences of Nucleophosmin Mutations in Acute Myeloid Leukemia. *J. Biol. Chem.* **2008**, 283, 23326-23332. (c) Döhner, K.; Schlenk, R.F.; Habdank, M.; Scholl, C.; Rücker, F.G.; Corbacioglu, A.; Bullinger, L.; Fröhling, S.; Döhner, H. Mutant nucleophosmin (NPM1) predicts favorable prognosis in younger adults with acute myeloid leukemia and normal cytogenetics: interaction with other gene mutations. *Blood.* **2005**, 106, 3740-3746.
- (19) (a) Chaudhuri, A.R.; Nussenzweig, A. The multifaceted roles of PARP1 in DNA repair and chromatin remodeling. *Nat. Rev. Mol. Cell Biol.* **2017**, 18, 610-621. (b) Langelier, M-F.; Pascal, J.M. PARP-1 mechanism for coupling DNA damage detection to poly(ADP-ribose) synthesis. *Curr. Opin. Struct. Biol.* **2014**, 23, 134-143. (c) Langelier, M-F.; Plank, J.L.; Pascal, J.M. Structural Basis for DNA Damage-Dependent Poly(ADP-ribosyl)ation by Human PARP-1. *Science.* **2012**, 336, 728-732. (d) Steffen, J.D.; Tholey, R.M.; Langelier, M-F.; Planck, J.L.; Schiewer, M.J.; Lal, S.; Bildzukewicz, N.A.; Yeo, C.J.; Knudsen, K.E.; Brody, J.R.; Pascal, J.M. Targeting PARP-1 Allosteric Regulation Offers Therapeutic Potential against Cancer. *Cancer Res.* **2014**, 74, 31-37.
- (20) Tien, M.Z.; Meyer, A.G.; Sydykova, D.K.; Spielman, S.J.; Wilke, C.O. Maximum Allowed Solvent Accessibilites of Residues in Proteins. *PLoS One* / **2013**, 8, e80635.
- (21) (a) Deng, H.; Gao, K.; Jankovic, J. The role of *FUS* gene variants in neurodegenerative diseases. *Nat. Rev. Neurology.* **2014**, 10, 337-348. (b) Loughlin, F.E.; Lukavsky, P.J.; Kazeeva, T.; Reber, S.; Hock, E-M.; Colombo, M.; Von Schroetter, C.; Pauli, P.; Cléry, A.; Mühlemann, O.; Polymenidou, M.; Ruepp, M-D.; Allain, F.H.-T. The Solution Structure of FUS Bound to RNA Reveals a Bipartite Mode of RNA Recognition with Both Sequence and Shape Specificity. *Mol Cell.* **2019**, 73, 490-504.
- (22) Kotani, T.; Sutomo, R.; Sasongko, T.H.; Gunadi, A.H.S.; Minato, T.; Fujii, E.; Endo, S.; Lee, M.J.; Ayaki, H.; Harada, Y.; Matsuo, M.; Nishio, H. A novel mutation at the N-terminal of SMN Tudor domain inhibits its interaction with target proteins. *J. Neurol.* **2007**, 254, 624-630.
- (23) Metodiev, M.D.; Thompson, K.; Alston, C.L.; Morris, A.A.M.; He, L.; Assouline, Z.; Rio, M.; Bahi-Buisson, N.; Pyle, A.; Griffin, H.; Siira, S.; Filipovska, A.; Munnich, A.; Chinnery, P.F.; McFarland, R.; Rötig, A.; Taylor, R.W. Recessive Mutations in *TRMT10C* Cause Defects in Mitochondrial RNA Processing and Multiple Respiratory Chain Deficiencies. *Am. J. Hum. Genet.* **2016**, 98, 993-1000.

Insert Table of Contents artwork here

